



The influence of addition of iridium-oxide to nickel-molybdenum-oxide cathodes on the electrocatalytic activity towards hydrogen evolution in acidic medium and on the cathode deactivation resistance

Abraham Gomez Vidales^{*}, Liem Dam-Quang, Anlan Hong, Sasha Omanovic

Department of Chemical Engineering, McGill University, 3610 University St., Montreal, Quebec, H3A 0C5, Canada

ARTICLE INFO

Article history:

Received 17 November 2018

Received in revised form

5 January 2019

Accepted 6 February 2019

Available online 7 February 2019

Keywords:

Hydrogen

Water electrolysis

Nickel

Molybdenum

Iridium

Metal oxides

Cathodes

Deactivation/reactivation

ABSTRACT

The influence of addition of Ir-oxide into Ni-Mo-oxide cathodes on the electrocatalytic activity of the hydrogen evolution reaction in acidic media was investigated. It was found that as the Ir-oxide content increased, the electrocatalytic activity towards hydrogen evolution also increased. This was attributed to the following two effects: the increase in the number of Ir surface sites and to the possible modification of the electronic structure of the material. Long-term electrolysis experiments confirmed high deactivation resistance of the Ni-Mo-Ir-oxide cathodes. It was also demonstrated that it is possible to *in-situ* reactivate the electrodes, making them potentially good cathode candidates for water electrolysis in the acidic medium.

© 2019 Elsevier Ltd. All rights reserved.

1. Introduction

In light of the environmental and geopolitical impacts of the fossil fuel-based energy systems, the need for a renewable energy economy is stronger than ever [1]. Hydrogen is increasingly being considered as an alternative medium of energy storage and production due to its lack of carbon dioxide emissions when produced through water electrolysis. However, in order to become economically competitive, commercial-scale hydrogen production costs must be further reduced, with the U.S. Department of Energy targeting a 50% reduction in production costs per kg by 2020 compared to 2015 [2]. Hydrogen can be produced in electrolyzers by splitting water through the hydrogen evolution reaction (HER) at the cathode. If the electricity used to drive these reactions is generated from a carbon-neutral source, then hydrogen can be created and stored without any significant greenhouse gas emissions.

^{*} Corresponding author.

E-mail address: abraham.gomezvidales@mail.mcgill.ca (A.G. Vidales).

The catalyst of choice for electrochemical hydrogen evolution is Pt, due to its high catalytic activity and stability [3,4]. Nevertheless, the use of Pt introduces high investment costs, due to the high price of the metal. Additionally, Pt tends to deactivate in acidic conditions, such as those found in proton exchange membrane (PEM) water electrolyzers, which are increasingly being considered as the technology of choice for water electrolysis [5]. The main advantages of PEM electrolysis over the conventional alkaline electrolysis (in which nickel and its alloys are used as the cathode) are the much higher current densities ($1\text{--}3\text{ A cm}^{-2}$ compared to 0.2 A cm^{-2}), the more significant energy efficiency of the process, and the purity of the produced hydrogen [6,7]. Moreover, PEM electrolyzers can work at higher (differential) pressures, allowing internal compression of the hydrogen required for its transport. Hence, PEM electrolyzers are ideal for small and remote plants and households with low and erratic energy consumption [8].

In the search for new materials and their applications, recent research studies and patents have claimed good performances of oxide electrodes for the cathodic evolution of hydrogen [6,7,9–13]. The reported advantage of such electrodes is that, unlike their

metallic counterparts, they are much less prone to poisoning by (underpotential) deposition of metals present as impurities in the electrolytes [11,14]. The effectiveness of transition metal oxides (TMOs) as catalysts for the HER was first reported in the 1980s [14]. Transition metal oxides have since emerged as one of the leading alternatives to noble metal electrodes. Although not as suitable as pure metals due to their lower activity, oxides are notable for being highly stable, even in harsh operating conditions. For example, there are few publications on the performance of iridium oxide (IrO_2) as a cathode. IrO_2 exhibits excellent corrosion resistance, excellent electrical conductivity, and high electrocatalytic activity toward hydrogen evolution reaction [9,11,15]. Furthermore, IrO_2 is widely used in the preparation of mixed oxide electrodes [11,16–18]. Despite its widespread use as a component of oxide electrodes in technological applications, no recent information whatsoever is available on the performance of iridium oxide as a cathode.

Given the number of advantages of PEM water electrolyzers over currently-used alkaline electrolyzers and considering that expensive Pt is still being used as a cathode in PEM electrolyzers, there is a strong incentive to replace Pt by cheaper electrocatalyst materials, while still maintaining high electrocatalytic activity and improving the deactivation resistance of the cathode [19–21]. Previous studies have demonstrated that Ni-Mo oxides can be used as cost-effective electrocatalysts for the HER [12]. Adding Ir to these mixtures could potentially increase the catalytic performance while remaining economically competitive. In this research paper, we present initial results on the effect of the addition of Ir to $\text{Ni}_{0.6}\text{-Mo}_{0.4}$ -oxide on the resulting HER kinetics and deactivation/reactivation of the electrodes. $\text{Ni}_{0.6}\text{-Mo}_{0.4}$ -oxide was chosen as the base cathode material since our previous results [12] demonstrated that this Ni/Mo ratio yielded the highest electroactivity in the HER in the acidic medium among the investigated Ni/Mo-oxide compositions.

2. Experimental procedure

2.1. Electrode preparation

The electrodes were prepared by coating titanium buttons (1.27 cm diameter, 0.2 cm thickness, purity 99.2%, Alfa Aesar, USA) with a metal oxide coating using a thermal-salt-decomposition method. Nickel, molybdenum, and iridium precursor solutions were prepared from dissolving salts $\text{NiCl}_2 \times 6\text{H}_2\text{O}$ (purity 99.9%, Sigma-Aldrich, Canada), $\text{Na}_2\text{MoO}_4 \times 2\text{H}_2\text{O}$ (purity 99.5 wt%, Sigma-Aldrich, Canada) and $\text{IrCl}_3 \times 3\text{H}_2\text{O}$ (purity 99.9 wt%, Sigma-Aldrich, Canada) in a mixture of 50 vol% HCl (37 wt%, Fisher Scientific, Canada) and 50 vol% nanopure water (resistivity 18.2 $\text{M}\Omega\text{ cm}$). Titanium buttons were polished to a uniform finish using 600 grit sandpaper, followed by etching in the boiling HCl solution of the concentration quoted above for 30 min and drying with argon gas (MEGS Specialty Gases Inc., 99.998 wt% pure, Canada). Nickel and molybdenum salts were mixed in a 60:40 molar metal-based ratio, while the percentage of iridium was varied with each set of samples, from 2 up to 60 mol.%. A 100% iridium-oxide electrode was also prepared. The analysis by electron dispersive spectroscopy (EDS) confirmed that the actual surface composition of the coatings was very similar to the nominal composition and that the elements were homogeneously distributed on the surface of the coatings. For comparison purposes, a flat Ni (purity: 99.9%) foil was used as a control cathode.

The Ti buttons were coated on one side with the prepared solution of the desired composition using standard paint brushes. After applying the metal-precursor solution on the Ti surface, the samples were first dried in an oven to 368 K for five minutes to

evaporate the solvent and subsequently transferred into a furnace to 773 K for fifteen minutes. The samples were then removed and allowed to cool at room temperature for ten minutes. Next, another coating layer was applied, and the process was repeated five times, for a total of six coatings. After applying the final coat, the buttons were kept in the furnace for one hour to convert metals into their oxides. Finally, the back side of the buttons was polished using 600 grit sandpaper to serve as the contact for the electrical circuit.

2.2. Physical characterization

The surface structure, composition, and morphology of the electrodes were studied by X-ray diffraction (XRD), electron dispersive spectroscopy (EDS), scanning electron microscopy (SEM) and stylus profilometry. The XRD patterns were recorded with a D8 Discover Bruker 2 Theta X-ray diffractometer equipped with a Cu source. The diffraction data were collected over an angle range of $2\theta = 20\text{--}90$ using GADDS software. The XRD generator was operated at 40 kV and 30 mA. The surface roughness was measured using a DektakXT stylus (Bruker, USA) surface profilometer. The measured area was $0.8\text{ mm} \times 1.5\text{ mm}$, and three measurements were conducted for an average value. SEM/EDS measurements were performed on a Hitachi SU-3500 Variable Pressure SEM (Hitachi, Japan) microscope (software: PC_SEM) with EDS detector (software: AZtecEnergy EDS).

2.3. Electrochemical characterization

Electrochemical techniques of Tafel polarization (TP), chronoamperometry (CA), chronopotentiometry (CP) were done to evaluate the performance of the electrodes in the HER, while electrochemical impedance spectroscopy (EIS) was used to measure the electrolyte resistance for the jR -drop correction and to obtain the real electrochemically-active surface area (EASA). These experiments were carried out using a typical three-electrode cell at room temperature $293 \pm 2\text{ K}$ and atmospheric pressure. The working electrode (WE) had a geometrical area of 0.68 cm^2 . A graphite rod was used as the counter electrode (CE), and it was placed inside a glass frit (Ace Glass Inc., USA) to avoid interfering with the HER. A saturated calomel electrode (SCE) (Accumet electrode, Fisher Scientific, USA) was used as the reference electrode (RE). The acidic electrolyte was prepared with H_2SO_4 (96 wt% pure, Fisher Scientific, Canada), and nanopure water. The electrolyte in the cell was deaerated with argon for 30 min before measurements, and argon was passed over the top of the solution during the experiment to keep an oxygen-free electrolyte solution. Before each electrochemical TP and CA measurement, the electrode was stabilized at -1.0 V for 30 min and the polarization was then started in the positive-going direction followed by performing an EIS measurement at 0.45 V to determine resistance for the jR -drop correction. Data acquisition and analysis were carried out with a potentiostat/galvanostat Autolab PGSTAT30 with NOVA software (v. 2.1; Metrohm, Netherlands). All the potentials are given versus the SCE, and all the polarization curves were corrected for the jR -drop.

2.4. Deactivation and reactivation of the electrodes

The same standard three-electrode electrochemical cell described above was used for investigating the susceptibility of electrodes towards deactivation and their capability towards reactivation. However, in this case, a platinum/rhodium wire (composition Pt 95 wt% and Rh 5 wt%, 0.5 mm diameter) was used as the counter electrode (CE). The electrolyte solution used as reference was $0.5\text{ M H}_2\text{SO}_4$. All the solutions were prepared with nanopure water. Three metal-ion solutions with Cu or Fe or Cu + Fe

ions dissolved in 0.5 M H_2SO_4 were made to examine the degree of deactivation of the cathodes by these metals. Cu in the form of $\text{CuSO}_4 \times 5\text{H}_2\text{O}$ (98% pure Sigma-Aldrich, Canada) and Fe was introduced in the form of $\text{FeSO}_4 \times 7\text{H}_2\text{O}$ (99% pure, Sigma-Aldrich, Canada). The amount of dissolved Cu and Fe was 10 ppm, which is around 20 times higher than the concentration in the industrial electrolyzers (this was done to accelerate the deactivation process and make the deactivation condition harsher). The prepared solutions were sonicated for 30 min to enhance dissolution of the salts fully. After assembling the cell, argon gas was used to purge the solution for 30 min before any electrochemical measurements were taken and the solution was continued to be purged throughout the deactivation experiment.

The following methodology was executed in order to evaluate the effect of electrode deactivation (deposition of metals on the electrode surface) and its subsequent reactivation. First, the cathode was stabilized at a potential of -1.0 V in pure 0.5 M H_2SO_4 for 30 min. Next, EIS was done at 0.45 V to determine resistance for the jR -drop correction. After this, TP in the hydrogen evolution region was performed, which gave the result on the freshly-prepared electrode HER activity. Then, the electrode was transferred into the “contaminated” solution, and galvanostatic polarization was performed for 24 h at a constant current density of -100 mA cm^{-2} ; this resulted in the deactivation of the electrode due to deposition of Cu and/or Fe on its surface. Hereafter, the electrode was rinsed with nanopure water, followed by a TP measurement in pure 0.5 M H_2SO_4 in the hydrogen evolution region to assess the degree of electrode deactivation. Next, the electrode was reactivated by polarizing it galvanostatically in the anodic region at 100 mA cm^{-2} for 30 min in pure 0.5 M H_2SO_4 . Finally, TP was repeated in a freshly-prepared pure 0.5 M H_2SO_4 solution to assess the degree of reactivation of the electrode, followed by an EIS measurement needed for the jR -drop correction.

In order to determine the influence of reactivation on the dissolution of Cu, Fe, Ni, Mo, and Ir, the electrolyte solution after reactivation was analyzed using a TraceScan Inductively Coupled Plasma – Optical Emission Spectroscopy (ICP-OES, iCAP 6500 dual view, Thermo Scientific, USA) system. The instrument was calibrated prior to the measurements using the standard solutions of the above-specified elements.

3. Results and discussion

3.1. Electrocatalytic activity in the HER

In order to evaluate the relative electrocatalytic activity of the produced electrode compositions in the HER, Tafel polarization curves were recorded. For comparison, the response of pure Ir-oxide and pure metallic Ni is also shown in Fig. 1a. Furthermore, steady-state polarization curves obtained from CA measurements are also presented in Fig. 1b, for comparison and validation purposes. The agreement between both sets of curves employing two different electrochemical techniques is excellent. These curves show the relationship between the overpotential (energy input) versus the current density (amount of hydrogen produced obtained through the Faraday law). As expected, with an increase in Ir content in the Ni-Mo-oxide coating, the hydrogen evolution current at a constant potential also increases. It is also important to mention that all the oxide-based electrodes display a significantly higher catalytic activity than pure metallic Ni, currently used in alkaline electrolyzers as a cathode (note that the results in Fig. 1 were recorded in an acidic medium, and the Ni curve is shown only for comparison purposes, despite this metal not being used in PEM electrolyzers). In addition, the HER onset potential decreased appreciably on the oxide electrodes in comparison to pure metal nickel.

As it can be seen in Fig. 1, the polarization curves corresponding to the response of electrodes that contain iridium deviate from the common Tafelian behavior (there is no defined linear Tafel region) and a semi-plateau region is reached at relatively low overpotential values. This effect can be attributed to the gradually-increasing electrode surface blockage by generated hydrogen bubbles (bubbles stick on the surface, reducing the electrochemically active surface area), and/or to the formation of hydrides on the surface layer (which can modify the electronic and structural properties of the coating) and/or to a local increase in pH at the electrode/electrolyte interface [15]. These results are similar to the ones from literature data reported recently for pure and other mixed Ir-oxide prepared by thermal decomposition [7,8,22].

A convenient way of evaluating the electrocatalytic activity of HER cathodes is by comparing the current density at a given overpotential. In the current case, this was done at an overpotential of -200 mV, and the results are presented in Fig. 2 using data obtained from TP and CA measurements.

When comparing the HER activity of pure Ir, Ni, and Mo metals,

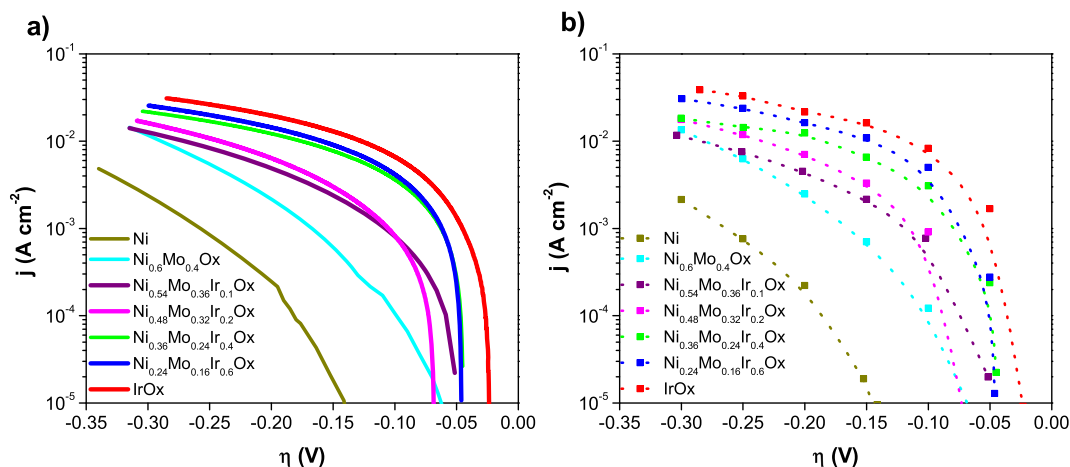


Fig. 1. a) Tafel polarization curves recorded in the hydrogen evolution region in 0.5 M H_2SO_4 on selected electrodes. Scan rate was 10 mVs^{-1} , b) Steady-state polarization curves recorded under the same conditions employing potentiostatic (CA) measurements.

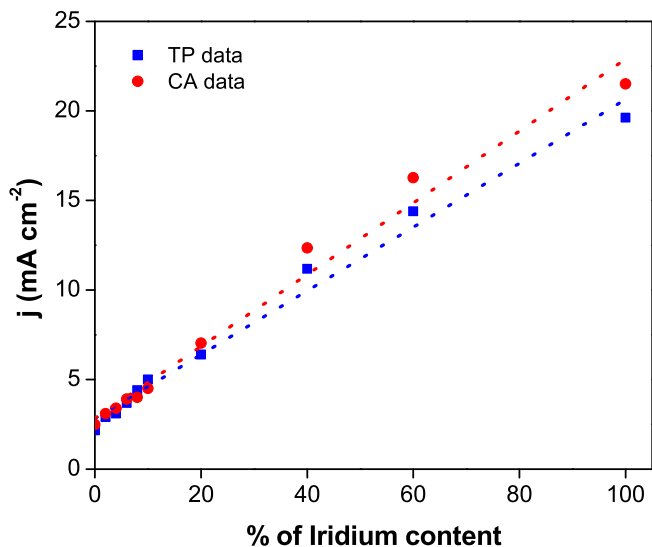


Fig. 2. Dependence of hydrogen evolution current density recorded at an overpotential of -200 mV as a function of iridium content in the metal-oxide electrode.

Ir sits on top of the HER volcano curve, two orders of magnitude higher than Ni and four orders of magnitude above Mo [23]. Although the electrodes investigated here are not pure metals, but rather their oxides, it could still be expected from Ir-oxide to offer higher HER electrocatalytic activity than the Ni-Mo-oxide electrode. The result in Fig. 2 shows that this is, indeed, the case. With an increase in Ir content in the Ni-Mo-oxide, the activity towards hydrogen evaluation increases linearly. Considering that these electrodes are much more complex than pure metal electrodes, the fundamental explanation for the trend observed in Fig. 2, based on the electrode (metal-oxide)-hydrogen bond strength only (volcano curve [23]), cannot be employed here. The linear trend indicates that the HER kinetics are, at least to a certain extent, proportional to the number of Ir-oxide active sites on the electrode surface.

3.2. Morphology and surface roughness of the electrodes

Fig. 3 shows the SEM images of the selected cathodes investigated in this work. The micrographs suggest that addition of Ir to the Ni-Mo-oxide results in a change in the surface morphology of the coating. While the surface that does not contain Ir (Fig. 3a)

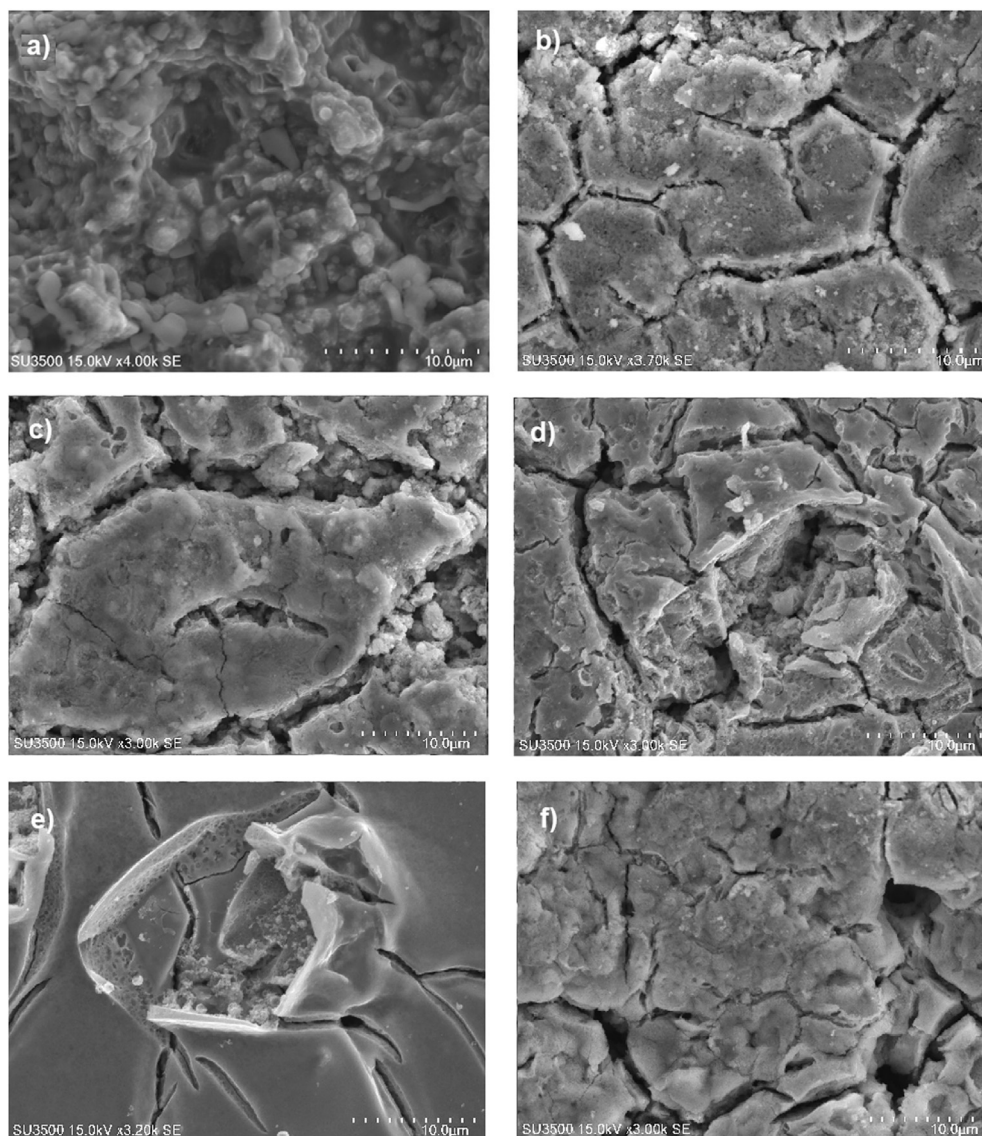


Fig. 3. SEM images of a) $\text{Ni}_{0.6}\text{Mo}_{0.4}$ -oxide, b) $\text{Ni}_{0.54}\text{Mo}_{0.36}\text{Ir}_{0.1}$ -oxide, c) $\text{Ni}_{0.48}\text{Mo}_{0.32}\text{Ir}_{0.2}$ -oxide, d) $\text{Ni}_{0.36}\text{Mo}_{0.24}\text{Ir}_{0.4}$ -oxide, e) $\text{Ni}_{0.24}\text{Mo}_{0.16}\text{Ir}_{0.6}$ -oxide, and f) Ir-oxide coating. The overall scale length on the images is $10\ \mu\text{m}$.

shows a porous structure characterized by globules of ca. 1–3 μm in diameter, the surfaces that contain Ir (Fig. 3b–f) display a cracked-mud morphology, which is characteristic of most metal-oxide coatings produced by thermal decomposition of their salts. This surface morphology is very similar to those observed with Ir, and Ir-oxide surfaces reported in the literature [24,25]. It was determined that the average thickness of the metal-oxide coatings is $5 \pm 2 \mu\text{m}$.

Next, the surface roughness, in this case, the arithmetic average of the roughness profile, R_a (μm), was determined using a stylus profilometer, and the values are presented in Table 1. The control surface, a flat metallic nickel plate, was characterized by the lowest surface roughness value. Producing an oxide electrode resulted in an increase in surface roughness; the base electrode material, $\text{Ni}_{0.6}\text{Mo}_{0.4}$ -oxide, displayed a surface roughness roughly twice of that presented by the metallic nickel plate. The addition of Ir into the metal oxide coating resulted in a further increase in surface roughness; with an increase in Ir content, the surface roughness, in general, also increases, indicating an increase in the surface area of the cathode available for the HER.

Next, in order to estimate the true electrochemically-active surface area (EASA) of the electrode exposed to the electrolyte, electrochemical impedance spectroscopy (EIS) measurements were performed [26]. Fig. S.1 in the supplementary material document shows an example of the EIS spectra recorded on the $\text{Ni}_{0.48}\text{Mo}_{0.32}\text{Ir}_{0.2}$ -oxide coating. The spectra were modeled using an electrical equivalent circuit (EEC) presented in Fig. S.2 in the supplementary material document. The agreement between the experimental (symbols) and modeled (line) data is good. The same procedure was employed to analyze spectra recorded on other electrode compositions, and the representative EEC parameters are listed in Table S.1. Then, using the Brug equation [26,27], Eq. S.1 in the supplementary material document, the electrode double layer capacitance was calculated, and the values are presented in Table 2. From this, the true electrochemically-active surface area (EASA) of the electrode was estimated by dividing these values by the theoretical electrochemical double-layer capacitance value of $20 \mu\text{F cm}^{-2}$. Similarly to the trend of surface roughness values in Table 1, the EASA values also increase with the increase in Ir content in the oxide coating. Both relative-increase trends (Tables 1 and 2) are linear, with the corresponding slopes of 0.056 ($R^2 = 0.961$) for

the surface roughness values, and 0.168 ($R^2 = 0.997$) for the EASA values. Given that profilometry can provide information only on the surface topography roughness at the micron scale, while EIS can provide information on the true electrochemically-active area that takes into account the coating porosity down to the nano-level, the relative comparison of the two slopes indicates that by increasing the Ir content in the oxide coating, the nano-level porosity increases significantly more than the micro-level surface roughness.

Taking into account the EASA values in Table 2, the linear trend in Fig. 2, which shows the extrinsic electrocatalytic activity of the cathodes, can be normalized for the surface-area effect to estimate the relative intrinsic activity of the catalysts. The resulting trend is presented in Fig. 4. With an increase in Ir content in the coating, the intrinsic activity of the cathode increases up to the Ir content of 40%, and then reaches a plateau. Although the trend is not linear as that one in Fig. 2, it still shows that the actual intrinsic HER activity of the cathodes depends strongly on the amount of Ir in the coating up to a certain relative Ir content (40%). The trends in Figs. 2 and 4 also indicate that the contribution to the intrinsic activity does not come only through the increase in Ir surface sites, but also through a possible modification of the electronic structure of the electrode; otherwise, the trend in Fig. 4 would be the same as that one in Fig. 2, taking into account that the Ir content on the top coating surface also increases in the same manner as that one in the bulk of the coating (which is the case, which has been verified by XPS – see Table S.2 in the supplementary material).

3.3. Structural characterization

The XRD patterns of selected electrodes are displayed in Fig. 5. From this analysis, in addition to the structure and composition of the coatings, the size of the crystals was estimated using the Scherrer equation $D = K\lambda/\beta\cos\theta$ where D is the mean size of the crystals, K is a dimensionless shape factor, (in this work $K = 0.9$), λ is the X-ray wavelength (in this work, $\lambda = 0.154 \text{ nm}$), β is the full width at half-maximum (FWHM) and θ is the Bragg angle [28,29].

The metallic Ni-control sample is presented as a reference, showing the corresponding characteristic phases of Ni at 44.5° , 51.6° , and 76.4° (JCPDS # 4–0835) and NiO at 37.1° and 43.3° , 61.1° (JCPDS # 78–0643), respectively and a crystalline structure. The

Table 1

Measured roughness of the surface electrodes Ni, Ni-Mo-oxide, and Ni-Mo-Ir-oxide.

Sample	Roughness R_a (μm)
Ni plate	0.26 ± 0.01
$\text{Ni}_{0.6}\text{Mo}_{0.4}\text{Ox}$	0.46 ± 0.02
$\text{Ni}_{0.54}\text{Mo}_{0.36}\text{Ir}_{0.1}\text{Ox}$	0.68 ± 0.05
$\text{Ni}_{0.48}\text{Mo}_{0.32}\text{Ir}_{0.2}\text{Ox}$	0.64 ± 0.07
$\text{Ni}_{0.36}\text{Mo}_{0.24}\text{Ir}_{0.4}\text{Ox}$	1.25 ± 0.11
$\text{Ni}_{0.24}\text{Mo}_{0.16}\text{Ir}_{0.6}\text{Ox}$	1.29 ± 0.13
IrOx	1.93 ± 0.10

Table 2

Double layer capacitance and electrochemically-active surface area of the investigated coatings obtained from the EIS data.

Sample	C_{DL} (F cm^{-2})	EASA (cm^2)
Ni	$(6.60 \pm 0.5) \times 10^{-5}$	3.3
$\text{Ni}_{0.6}\text{Mo}_{0.4}\text{Ox}$	$(4.20 \pm 0.7) \times 10^{-4}$	21
$\text{Ni}_{0.54}\text{Mo}_{0.36}\text{Ir}_{0.1}\text{Ox}$	$(5.85 \pm 0.3) \times 10^{-4}$	29
$\text{Ni}_{0.48}\text{Mo}_{0.32}\text{Ir}_{0.2}\text{Ox}$	$(6.48 \pm 0.5) \times 10^{-4}$	32
$\text{Ni}_{0.36}\text{Mo}_{0.24}\text{Ir}_{0.4}\text{Ox}$	$(8.96 \pm 1.6) \times 10^{-4}$	45
$\text{Ni}_{0.24}\text{Mo}_{0.16}\text{Ir}_{0.6}\text{Ox}$	$(1.12 \pm 0.6) \times 10^{-3}$	56
IrOx	$(1.54 \pm 0.9) \times 10^{-3}$	77

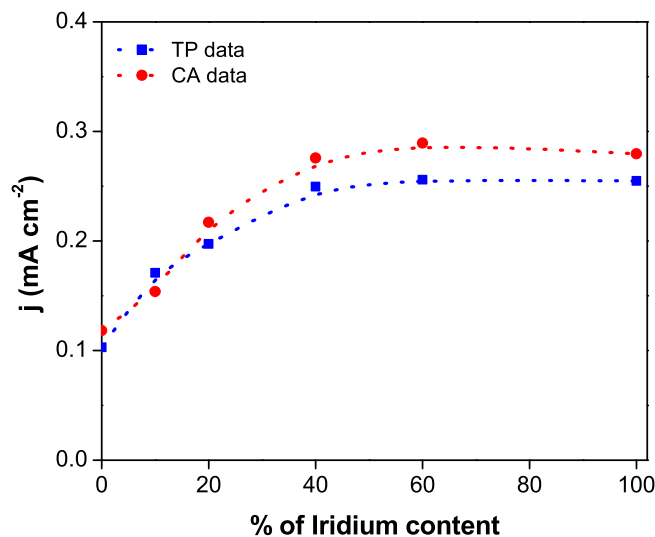


Fig. 4. Dependence of hydrogen evolution current density normalized by the true electrochemically-active surface area recorded at an overpotential of -200 mV as a function of iridium content in the metal-oxide electrode.

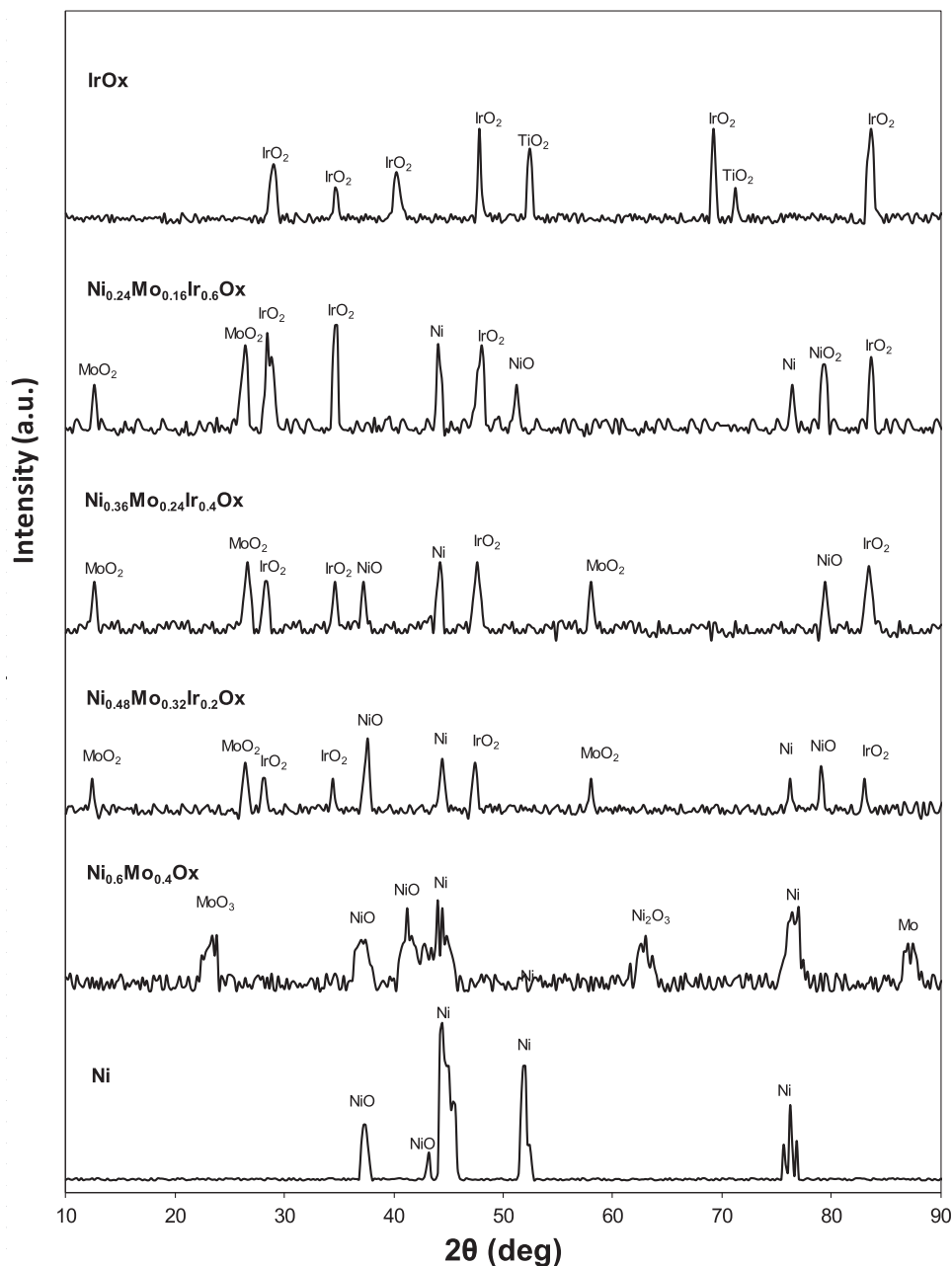


Fig. 5. XRD spectra of Ni, Ni-Mo-oxide and Ni-Mo-Ir-oxide coatings deposited on a titanium substrate.

intensity of the XRD peaks from metallic Ni is still relatively high after annealing, indicating that the bulk of the film is not entirely oxidized [15]. The base oxide material, $\text{Ni}_{0.6}\text{Mo}_{0.4}\text{-oxide}$, is also presented, exposing a more amorphous structure and the existence of peaks that could be assigned to Ni, NiO, Ni_2O_3 , Mo, and MoO_3 . In the case of the Ni-Mo-Ir-oxide coatings, the characteristic peaks of Ni, NiO, MoO_2 , and IrO_2 are visible, indicating that molybdenum and nickel oxidative states decreased from +6 to +4 and from +3 to +2, respectively, when the precursor Ir solution was incorporated into the coating. Furthermore, after adding Ir, the properties of the Ni-Mo coatings changed slightly, compared with that of the $\text{Ni}_{0.6}\text{Mo}_{0.4}\text{-oxide}$ coating. The addition of Ir to the Ni-Mo coating led to remarkably sharper and narrower defined peaks, indicating the formation of larger crystals specifically in the case of Ni, IrO_2 , and

MoO_2 (the average size of Ir increased from 14.5 nm to 23.5 nm when the Ir content increased from 10 to 60%, a less notorious increment from 12.3 nm to 18.4 nm occurred in the case of nickel for the same range) and a more defined crystalline structure [30]. Finally, the Ir-oxide sample contains rutile IrO_2 (JCPDS #15–870), and TiO_2 , and its structure is crystalline [31]. The presence of rutile TiO_2 (JCPDS # 88–1175) at 54.5° and 73.2° could be a consequence of the coating method whereby some Ti from the substrate diffused towards the outer coating surface, where it was detected by both XRD and EDS [31]. These results confirmed that the Ni-Mo-Ir-oxide coatings were successfully prepared by the thermal-salt decomposition method employed in this research.

3.4. Electrocatalytic stability of electrodes

It is expected from good electrocatalysts to yield stable performance over a long-term service. Although the goal of the current work was not to fabricate electrodes that would offer long-term stable electrocatalytic performance, but only to investigate the influence of addition of Ir into the Ni-Mo-oxide structure on the HER kinetics, it was interesting to examine the performance of the electrocatalysts over a four-day period of time of constant electrolysis of water. For this purpose, 40%, 60%, and 100% Ir-containing electrodes were tested by performing hydrogen production at a current density of -500 mA cm^{-2} for a period of 96 h in $0.5 \text{ M H}_2\text{SO}_4$. For comparison, the electrocatalytic performance of pure metallic nickel was also investigated.

During the electrolysis process at this high current density, the potential of the Ni-Mo-Ir-oxide electrodes did not change significantly indicating their stable electrocatalytic performance. Nevertheless, for metallic nickel, the cathodic overpotential increased substantially with time, evidencing deactivation of the cathode. On completion of the electrolysis experiment, Tafel polarization curves were recorded and compared with those recorded on the freshly-prepared electrodes, prior electrolysis, in order to calculate the percentage of remaining activity. These results are presented in Fig. 6. As it is seen, the electrocatalytic activity of metallic Ni decreased to half of the initial activity, ca. 53%, while the three Ir-containing oxide coatings kept the activity between 85% and 90% of the initial value. Since the electrodes were used as cathodes, the

loss in activity was most-likely due to their deactivation by deposition of trace metals present in the electrolysis electrolyte, rather than their corrosion/dissolution. These results indicate that the Ni-Mo-Ir-oxide coatings are less susceptible to deactivation, which makes them good candidates for HER in PEM electrolyzers.

Studies on the influence of impurities present in the electrolyte on the behavior of HER cathodes have been carried out at constant current densities [32–34], and it was found that there is a marked loss in electrocatalytic activity with time. Various impurities deposited on the cathode surface could also reduce the electrical conductivity of the electrode. Electrolytes used in industrial hydrogen-production processes usually contain dissolved metal ions, such as Cu, and Fe (around 0.5–1 ppm for each), which are gradually electrodeposited on the cathode and in that way affect the electrode performance in the HER [35].

The experiments presented in Fig. 6 show that there is a loss of activity during a four-day electrolysis period in $0.5 \text{ M H}_2\text{SO}_4$ electrolyte prepared using nanopure water, most likely due to the deactivation by impurities present in traces in the electrolyte. To more closely investigate the deactivation resistance of the prepared cathodes, a better-controlled set of deactivation experiments were performed and under much more severe conditions, followed by investigating the possibility of cathode reactivation.

The two most active Ni-Mo-Ir-oxides (corresponding to the samples 40% and 60% of Ir content), and the control nickel sample were deactivated by performing electrolysis at -100 A cm^{-2} for 24 h in the electrolyte containing 10 ppm Cu, or 10 ppm Fe, or 20 ppm Cu + Fe. The degree of electrode deactivation was calculated by comparing the hydrogen evolution current density at overpotentials of -150 , -200 and -250 mV before and after the deactivation, and the results are presented in Fig. 7a.

Nickel displays the weakest performance (largest degree of deactivation), similarly to the result in Fig. 6. In contrast, both metal oxide electrodes maintained a relatively high activity, evidencing their significantly higher resistance towards deactivation. The mechanism of deactivation is by electrodeposition of the metals on the cathode surface, effectively converting the Ni-Mo-Ir-oxide surface into Cu, Fe or Cu + Fe and thus altering the HER kinetics [34]. EDS confirmed the presence of Cu and Fe on the Ni-Mo-Ir-oxide surfaces. For the solution containing Cu, it was found that Cu almost entirely covered the surface of all the electrodes investigated. The thickness of the Cu layer was $10 \pm 2 \text{ nm}$. Furuya et al. [36] showed that by increasing Cu concentration in the electrolyte ($0.5 \text{ M H}_2\text{SO}_4$) up to $3 \times 10^{-6} \text{ mol L}^{-1}$, there was a significant decrease in the rate of hydrogen production on the Pt cathode. Cobourn et al. [34] obtained similar results increasing the

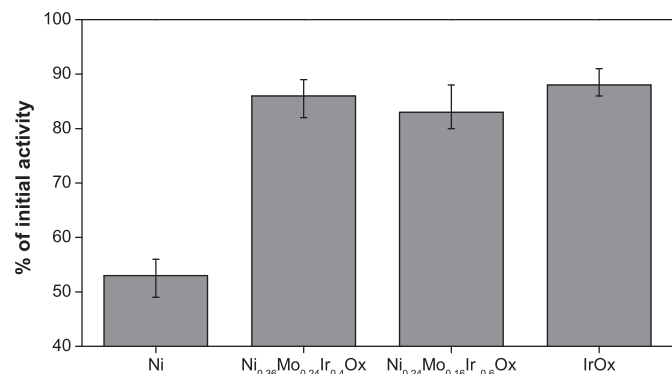


Fig. 6. Percentage of remaining electrocatalytic activity in the HER of selected electrodes measured at an overpotential of -150 mV in $0.5 \text{ M H}_2\text{SO}_4$ after 96 h of electrolysis at -500 mA cm^{-2} .

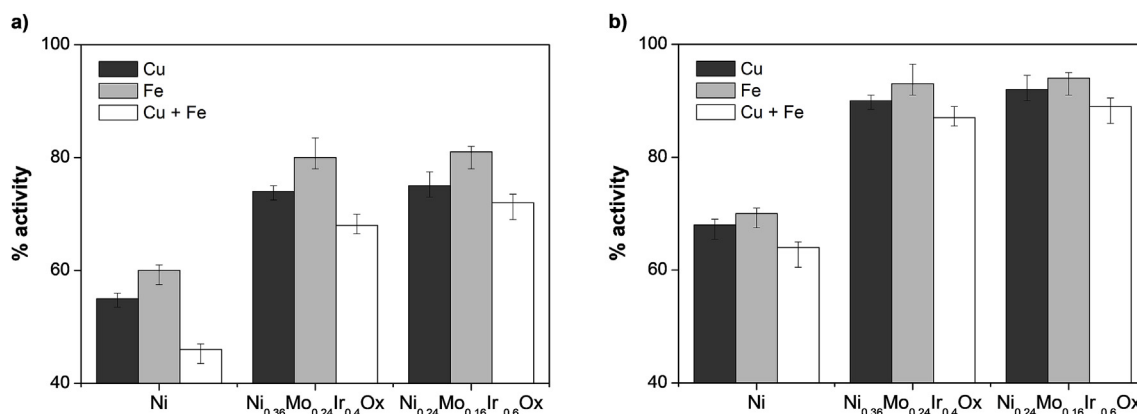


Fig. 7. a) Percentage of remaining electrocatalytic activity in the HER of selected electrodes after deactivation in $0.5 \text{ M H}_2\text{SO}_4$ containing 10 ppm of dissolved Cu, Fe or 20 ppm Cu + Fe. b) Percentage of restored initial electrocatalytic activity after applying an in-situ re-activation method.

concentration of Cu up to 10 ppm, and they found a 50% decrease of the current density in comparison with the pure electrolyte solution (0.5 M H₂SO₄) when Pt/C cathodes were employed.

In the case of the electrolyte containing Fe, the amount of Fe on the surface was lower, and Fe did not cover the whole cathode surface; the thickness of this layer was 5 ± 1 nm. This was reflected by a smaller degree of deactivation in comparisons to that one with Cu (Fig. 7a). In similar studies, but in alkaline media (employing an electrolyte solution of 30 wt% KOH at 343 K), Huot and Brossard [32] reported a decremental of the electrocatalytic activity on the nickel cathode when the solution contained 0.5 ppm Fe, based on the increase of the overpotential from -362 mV to -541 mV (an increment of around 50%) between a period of 60 s and 33.7×10^4 s at a constant current density of -250 mA cm⁻².

Finally, when the deactivation was done in the electrolyte containing both 10 ppm Cu and 10 ppm Fe, the degree of deactivation was more significant than that with Cu (Fig. 7a), which was to expect due to the higher total (sum) concentration of the two metals (20 ppm). EDS revealed that Cu was preferentially deposited on the surface, with a Cu + Fe ratio of 3/2. The preferential deposition of Cu is to expect since Cu has a more positive standard potential than Fe. The thickness of the bi-metal layer was found to be 13 ± 3 nm.

As it is inevitable for HER cathodes to deactivate with time, it would be desirable to re-activate them *in-situ*, rather than to either replace them or perform reactivation externally, which would require disassembly of the electrolyzer. A convenient way to perform *in-situ* reactivation would be to switch the electrolyzer polarity and dissolve metal (and other) impurities by anodic oxidation, flush out the dissolved impurities and continue with the electrolyzer operation by re-switching back the polarity. A simple simulation of this scenario was done in this research.

Namely, after deactivating the cathodes (Fig. 7a), they were then polarized in 0.5 M H₂SO₄ as anodes at 100 mA cm⁻² for 30 min, followed by testing of their HER activity in a fresh 0.5 M H₂SO₄ electrolyte by TP. The degree of electrode reactivation was then calculated by comparing the recorded hydrogen evolution current density at overpotentials of -150 , -200 and -250 mV to the values obtained with the freshly-prepared electrodes (before deactivation), and the results are presented in Fig. 7b. The reactivation procedure had the smallest effect on the Ni cathode, while the two Ni-Mo-Ir-oxide cathodes achieved ca. 90% of the original activity. It can be assumed that by optimizing the reactivation conditions (which was not the goal of this study), even a higher degree of reactivation could be achieved. Nonetheless, the experiments presented in Fig. 7 demonstrate that the Ni-Mo-Ir-oxide cathodes are significantly more resistant to deactivation than the Ni electrode and that it is possible to *in-situ* reactivate them, at least to a certain degree.

In order to investigate if the reactivation results in dissolution of Ni, Mo or Ir, ICP analysis of the spent reactivation H₂SO₄ electrolyte (after reactivation) was done; however, for these experiments in order to increase the concentration of dissolved elements, reactivation was done over a period of four hours, rather than over a period of 30 min as in the case of reactivation results presented in Fig. 7b. ICP analysis confirmed a significant increase in Cu, Fe, and Cu + Fe in the reactivation electrolyte as a result of dissolution of these metal impurities. No Ir was detected, while a negligible increase in Ni was detected (the Cu and Fe salts already contained trace amounts of Ni, and a relative increase in dissolved Ni by 4×10^{-8} wt% was detected as the consequence of reactivation). Mo was also detected at a very low concentration (5.61×10^{-6} wt %). This indicates that some negligible dissolution of Ni and Mo occurs during the reactivation procedure, which could potentially limit the applicability of the procedure over a longer period of time (higher

number of reactivation cycles). Nevertheless, the extrapolation of the reactivation single-period time (one four-hour cycle) to the same time length done over multiple reactivation cycles might not be straightforward as the initial dissolution of metals from the deactivated electrode occurs primarily through the dissolution of Cu and Fe, rather than that of Ni and/or Mo. Thus, further studies are needed for more conclusive data and to optimize the reactivation procedure (temperature, current density, time) in order to maximize the dissolution of Cu and Fe, and minimize degradation of the electrode through the dissolution of base Ni and Mo components.

4. Conclusion

The results demonstrate that the Ni-Mo-Ir-oxide cathodes prepared by thermal decomposition exhibit good performance for the HER in the acidic medium. The cathodes were found to be crystalline and exhibit a cracked-mud surface morphology of increasing surface roughness with Ir content increase. The electrochemical activity of the Ni-Mo-Ir-oxides was found to be dependent on the amount of Ir, which contributed to the increase in intrinsic activity due to both the increase in the number of Ir surface sites and possible modification of the electronic structure of the material. Long-term electrolysis experiments confirmed significantly higher fouling resistance of the oxide electrodes in comparison to the pure metal Ni electrode. It was also demonstrated that it is possible to *in-situ* reactivate all the electrodes; however, the degree of reactivation of Ni-Mo-Ir-oxide electrodes was found to be much higher. The results presented here show that Ni-Mo-Ir-oxide could represent good candidates for cathodes for water electrolysis in the acidic medium, potentially in PEM electrolyzers. Nevertheless, further investigation is needed in the direction of fabricating nanoparticulate Ni-Mo-Ir-oxide electrodes and investigating their performance in a real PEM cell.

Acknowledgment

Financial support from McGill University through the McGill Engineering Doctoral Award (MEDA) program, the Eugenie Ulmer Lamothe Endowment, the Natural Sciences and Engineering Research Council of Canada (NSERC), and the National Council of Science and Technology (CONACYT) is gratefully acknowledged.

Appendix A. Supplementary data

Supplementary data to this article can be found online at <https://doi.org/10.1016/j.electacta.2019.02.030>.

References

- [1] A. Energy Information, *International Energy Outlook*, vol.2016, 2016.
- [2] DOE Technical Targets for Hydrogen Production from Electrolysis | Department of Energy.
- [3] M.G. Walter, E.L. Warren, J.R. McKone, S.W. Boettcher, Q. Mi, E.A. Santori, N.S. Lewis, Solar water splitting cells, *Chem. Rev.* 110 (2010) 6446–6473.
- [4] S. Trasatti, Work function, electronegativity, and electrochemical behaviour of metals, *J. Electroanal. Chem. Interfacial Electrochem.* 39 (1972) 163–184.
- [5] S. Cherevko, G.P. Keeley, S. Geiger, A.R. Zeradjanin, N. Hodnik, N. Kulyk, K.J.J. Mayrhofer, Dissolution of platinum in the operational range of fuel cells, *ChemElectroChem* 2 (2015) 1471–1478.
- [6] P. Millet, M. Pineri, R. Durand, New solid polymer electrolyte composites for water electrolysis, *J. Appl. Electrochem.* 19 (1989) 162–166.
- [7] E. Rasten, G. Hagen, R. Tunold, Electrocatalysis in water electrolysis with solid polymer electrolyte, *Electrochim. Acta* 48 (2003) 3945–3952.
- [8] E. Slavcheva, I. Radev, S. Bliznakov, G. Topalov, P. Andreev, E. Budevski, Sputtered iridium oxide films as electrocatalysts for water splitting via PEM electrolysis, *Electrochim. Acta* 52 (2007) 3889–3894.
- [9] J. Boodts, S. Trasatti, Hydrogen evolution on iridium oxide cathodes, *J. Appl. Electrochem.* 19 (1989) 255–262.

- [10] L. Chen, D. Guay, A. Lasia, Kinetics of the hydrogen evolution reaction on RuO₂ and IrO₂ oxide electrodes in H₂SO₄ solution: an AC impedance study, *J. Electrochem. Soc.* 143 (1996) 3576–3584.
- [11] I. Kodintsev, S. Trasatti, Electrocatalysis of H₂ evolution on RuO₂+ IrO₂ mixed oxide electrodes, *Electrochim. Acta* 39 (1994) 1803–1808.
- [12] A.G. Vidales, S. Omanovic, Evaluation of nickel-molybdenum-oxides as cathodes for hydrogen evolution by water electrolysis in acidic, alkaline, and neutral media, *Electrochim. Acta* 262 (2018) 115–123.
- [13] A.G. Vidales, K. Choi, S. Omanovic, Nickel-cobalt-oxide cathodes for hydrogen production by water electrolysis in acidic and alkaline media, *Int. J. Hydrog. Energy* 43 (2018) 12917–12928.
- [14] E.R. Kötz, S. Stucki, Ruthenium dioxide as a hydrogen-evolving cathode, *J. Appl. Electrochem.* 17 (1987) 1190–1197.
- [15] S. Cherevko, S. Geiger, O. Kasian, N. Kulyk, J.-P. Grote, A. Savan, B.R. Shrestha, S. Merzlikin, B. Breitbach, A. Ludwig, Oxygen and hydrogen evolution reactions on Ru, RuO₂, Ir, and IrO₂ thin film electrodes in acidic and alkaline electrolytes: a comparative study on activity and stability, *Catal. Today* 262 (2016) 170–180.
- [16] E. Balko, P. Nguyen, Iridium-tin mixed oxide anode coatings, *J. Appl. Electrochem.* 21 (1991) 678–682.
- [17] M. Blouin, D. Guay, Activation of ruthenium oxide, iridium oxide, and mixed Ru/Ir-oxide electrodes during cathodic polarization and hydrogen evolution, *J. Electrochem. Soc.* 144 (1997) 573–581.
- [18] M.T. Reetz, M. Lopez, W. Grünert, W. Vogel, F. Mählendorf, Preparation of colloidal nanoparticles of mixed metal oxides containing platinum, ruthenium, osmium, and iridium and their use as electrocatalysts, *J. Phys. Chem. B* 107 (2003) 7414–7419.
- [19] M. Zeng, Y. Li, Recent advances in heterogeneous electrocatalysts for the hydrogen evolution reaction, *J. Mater. Chem.* 3 (2015) 14942–14962.
- [20] J. Garche, C.K. Dyer, P.T. Moseley, Z. Ogumi, D.A. Rand, B. Scrosati, *Encyclopedia of Electrochemical Power Sources*, Newnes, 2013.
- [21] P.P. Edwards, V.L. Kuznetsov, W.I. David, N.P. Brandon, Hydrogen and fuel cells: towards a sustainable energy future, *Energy Policy* 36 (2008) 4356–4362.
- [22] T. Pauporté, R. Durand, Impedance spectroscopy study of electrochromism in sputtered iridium oxide films, *J. Appl. Electrochem.* 30 (2000) 35–41.
- [23] S. Trasatti, Work function, electronegativity, and electrochemical behaviour of metals: III. Electrolytic hydrogen evolution in acid solutions, *J. Electroanal. Chem. Interfacial Electrochem.* 39 (1972) 163–184.
- [24] F. Lei, Y. Sun, K. Liu, S. Gao, L. Liang, B. Pan, Y. Xie, Oxygen vacancies confined in ultrathin indium oxide porous sheets for promoted visible-light water splitting, *J. Am. Chem. Soc.* 136 (2014) 6826–6829.
- [25] G. Topalov, G. Ganske, E. Lefterova, U. Schnakenberg, E. Slavcheva, Preparation and properties of thin Pt–Ir films deposited by dc magnetron co-sputtering, *Int. J. Hydrog. Energy* 36 (2011) 15437–15445.
- [26] E. Navarro-Flores, Z. Chong, S. Omanovic, Characterization of Ni, NiMo, NiW and NiFe electroactive coatings as electrocatalysts for hydrogen evolution in an acidic medium, *J. Mol. Catal. Chem.* 226 (2005) 179–197.
- [27] G. Brug, A. Van Den Eeden, M. Sluyters-Rehbach, J. Sluyters, The analysis of electrode impedances complicated by the presence of a constant phase element, *J. Electroanal. Chem. Interfacial Electrochem.* 176 (1984) 275–295.
- [28] D. Xu, P. Diao, T. Jin, Q. Wu, X. Liu, X. Guo, H. Gong, F. Li, M. Xiang, Y. Ronghai, Iridium oxide nanoparticles and iridium/iridium oxide nanocomposites: photochemical fabrication and application in catalytic reduction of 4-nitrophenol, *ACS Appl. Mater. Interfaces* 7 (2015) 16738–16749.
- [29] A. Monshi, M.R. Foroughi, M.R. Monshi, Modified Scherrer equation to estimate more accurately nano-crystallite size using XRD, *World J. Nano Sci. Eng.* 2 (2012) 154–160.
- [30] H. Xue, C. Wei, N. Ping, S.-z. LUO, T. ZHANG, Promoting effects of iridium on nickel based catalyst in ammonia decomposition, *J. Fuel Chem. Technol.* 35 (2007) 691–695.
- [31] A. Battisti, X-ray diffraction characterization of iridium dioxide electrocatalysts, *J. Mater. Chem.* 1 (1991) 511–515.
- [32] J. Huot, L. Brossard, Time dependence of the hydrogen discharge at 70 °C on nickel cathodes, *Int. J. Hydrog. Energy* 12 (1987) 821–830.
- [33] L. Brossard, J.-Y. Huot, Influence of iron impurities on the time dependence of the hydrogen evolution reaction on platinum cathodes during electrolysis of 30 w/o KOH, *J. Appl. Electrochem.* 19 (1989) 882–888.
- [34] S.L. Cobourn, E.B. Easton, The effect of copper contamination at the cathode of Cu-Cl/HCl electrolyzers, *Int. J. Hydrog. Energy* 42 (2017) 28157–28163.
- [35] L. Brossard, Electrocatalytic performance for alkaline water electrolysis of Ni electrodes electrocoated with Fe or Fe/Mo, *Int. J. Hydrog. Energy* 16 (1991) 13–21.
- [36] N. Furuya, S. Motoo, The electrochemical behavior of ad-atoms and their effect on hydrogen evolution: Part I. Order-disorder rearrangement of copper ad-atoms on platinum, *J. Electroanal. Chem. Interfacial Electrochem.* 72 (1976) 165–175.